Science Bulletin 64 (2019) 808–813

Contents lists available at ScienceDirect

Science Bulletin

journal homepage: www.elsevier.com/locate/scib

Science Bulletin
www.scibull.com

Article

Asymmetric transmission of acoustic waves in a waveguide via gradient index metamaterials

Wen-Kang Cao [a], Li-Ting Wu [a], Cheng Zhang [a], Jun-Chen Ke [a], Qiang Cheng [a,*], Tie-Jun Cui [a,*], Yun Jing [b,*]

[a] State Key Laboratory of Millimeter Waves, Department of Radio Engineering, Southeast University, Nanjing 210096, China
[b] Department of Mechanical and Aerospace Engineering, North Carolina State University, Raleigh, NC 27695, USA

ARTICLE INFO

Article history:
Received 30 October 2018
Received in revised form 12 December 2018
Accepted 25 December 2018
Available online 6 January 2019

Keywords:
Asymmetric transmission
Surface waves
Gradient index metamaterials
Waveguide

ABSTRACT

We demonstrate that asymmetric acoustic wave transmission in a waveguide can be achieved via gradient index metamaterials (GIMs). We theoretically prove that the acoustic wave can be efficiently converted to surface waves (SWs) via GIMs. The GIMs in a waveguide can allow the transmission of acoustic waves in one direction but block them in the other direction. This theory is validated by experiments. Our findings may provide new applications in various scenarios such as high-efficiency acoustic couplers and noise control.

1. Introduction

Acoustic metamaterials and metasurfaces have shown great flexibility to control the behaviors of sound. Many significant research efforts have been demonstrated, including the works on negative refraction [1–3], noise control [4,5], hyperlens [6], diffusers [7,8] and other acoustic devices [9,10]. Asymmetric transmission of acoustic waves, on the other hand, is a phenomenon where sound is permitted to transmit in one direction, but not the other. It has been realized through active systems [11]. For example, Gu et al. [12] designed an acoustic diode by using an acoustic nonlinear material and a pair of gain and lossy materials. Popa et al. [13] demonstrated a non-reciprocal active system to achieve the unidirectional acoustic energy transmission which consists of a piezoelectric membrane connected with a circuit. Although active systems could demonstrate large asymmetrical effects, they have many disadvantages, such as their complexity and inevitable energy consumption.

In order to overcome the limitations of active systems, a variety of passive structures have been investigated, such as asymmetric acoustic gratings [14,15], lossy metasurfaces [16], and cascaded metasurfaces [17,18] and the other acoustic devices [19–21]. Although extensive works have been carried out in this area, new design schemes are still in need for the sake of more robust asymmetric sound transmission. Recently, there has been a growing interest in researching the conversion of propagating waves to surface waves (SWs) [22,23]. For instance, electromagnetic (EM) wave gradient index metamaterials (GIMs) have been theoretically and experimentally demonstrated for nearly perfect conversion of propagating waves to SWs [24]. It is further shown that such a wave mode conversion can be utilized for unidirectional transmission [25]. As the counterpart of EM waves, it is expected that acoustic waves can also be manipulated in a similar fashion. However, to the best of our knowledge, this scheme has not been demonstrated in acoustics.

In this letter, we investigate an acoustic wave structure consisting of a pair of two-dimensional GIMs symmetrically distributed in a waveguide. The GIMs are realized by unit cells with rotational symmetry. When the incoming acoustic wave propagates along the direction where the relative index increases, the acoustic wave is converted to SWs and is allowed to transmit in this direction. For the opposite direction, where the relative index decreases, the sound is blocked, giving rise to asymmetric acoustic wave transmission. Numerical simulations and experiments are provided to validate the proposed design.

2. Theory and design

2.1. Conceptual design

Fig. 1a shows the schematic diagram of the two-dimensional (2D) asymmetric acoustic wave transmission system. It consists

SPECIAL TOPIC: Electromagnetic Metasurfaces: from Concept to Applications.

* Corresponding authors.
E-mail addresses: qiangcheng@seu.edu.cn (Q. Cheng), tjcui@seu.edu.cn (T.-J. Cui), yjing2@ncsu.edu (Y. Jing).

https://doi.org/10.1016/j.scib.2019.01.002
2095-9273/

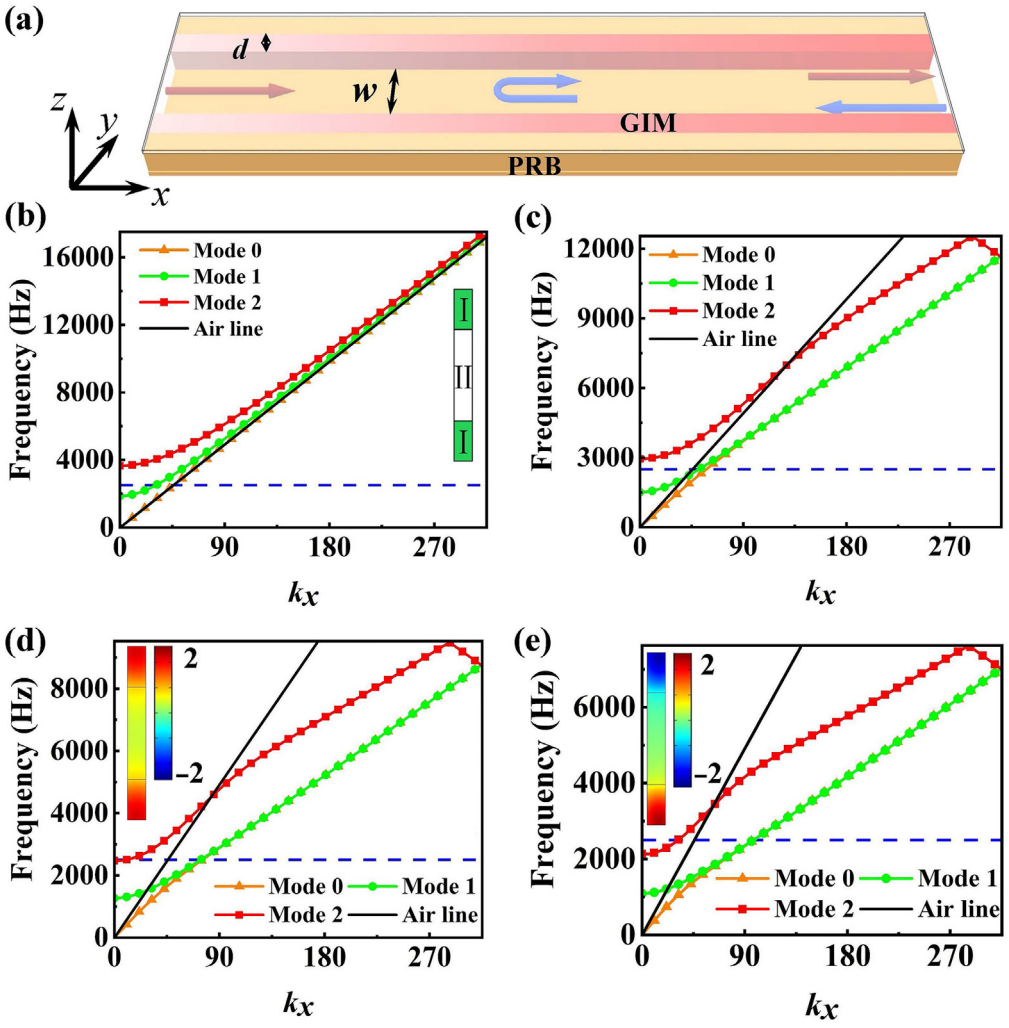

Fig. 1. The schematic diagram of a waveguide with GIMs and the dispersion of the unit cell. (a) Schematic diagram of asymmetric acoustic waves transmission system. The gradually changing red regions represent the relative refractive indices of the GIMs gradually increase from left to right. The background media is air and the outside boundaries of the waveguide are the perfect rigid boundary. The arrows show the acoustic wave propagation directions from the left port (red arrows) and the right port (blue arrows). (b)–(e) The dispersion relations of the ideal unit cell of the waveguide with the GIMs. The inset in (b) is the ideal unit cell, which the region I is the effective media with the relative refractive index 1 (b), 1.5 (c), 2 (d) and 2.5 (e), respectively. The insets in (d)–(e) show the eigenmode fields of the mode 0 and mode 1 at 2,500 Hz. The black lines are the air line and the blue dash lines indicate the working frequency 2,500 Hz.

of a waveguide and two GIMs mounted on the inner walls of the waveguide. The gradually changing red regions represent the relative refractive index of the GIMs, which slowly increases in the direction pointing to the right. The relative refractive index of the GIMs is governed by the following equation [25]:

$$n(x) = 1 + \frac{kx}{2k_0 d}, \tag{1}$$

where k is the increasing rate of the relative refractive index, k_0 is the wavenumber of the background medium (air), and d is the thickness of the GIMs. The width of the waveguide is denoted as w and the waveguide is enclosed by perfect rigid boundaries (PRBs). The relative refractive index of the GIMs provides a gradient phase shift as

$$\varphi(x) = \varphi_0 + kx, \tag{2}$$

where φ_0 is the initial phase. When the acoustic wave is incident from the left, it propagates inside the waveguide while interacting with the GIMs. The GIMs provide a gradient phase shift along the interface between the GIMs and air, and finally cause the acoustic wave to be converted into SWs and transmitted to the right port (red arrows). For the acoustic wave traveling to the right, the gradient phase shift is flipped, and the acoustic wave stops propagating at a certain location in the waveguide (blue arrows), for the reason that will be explained in details below.

The mechanism of this asymmetric wave propagation phenomenon can be unveiled by investigating the dispersion relations of the waveguide using a commercial software package (COMSOL Multiphysics 5.3a). In order to simulate the dispersion relations, we build an ideal unit cell (the inset in Fig. 1b) with the period p = 10 mm, which is consistent with the real-structure unit cell as shown below. Here, region I is the effective medium with a constant relative refractive index and the region II is air. The periodic boundary condition is chosen for the left and right boundaries and the top and bottom boundaries are acoustically hard. We choose the dimensions as d = 22 mm and w = 50 mm. In Fig. 1b–e, the relative refractive index of region II gradually changes from 1 to 2.5 as increment of 0.5. The black lines are air lines and the blue dash lines indicate the frequency of 2,500 Hz. Dispersion curves for the 3 lowest modes (mode 0, 1, and 2) are plotted. When the incident acoustic wave comes from the left, the relative refractive

index of the effective media slowly increases from 1 to a higher value. Fig. 1b indicates that the dispersion curves of mode 0, mode 1 and mode 2 are on the left side of the air line when the relative refractive index is 1. Consequently, acoustic waves cannot be converted to SWs [26]. On the other hand, in Fig. 1c–e, the dispersion curves of mode 0 and mode 1 are mostly on the right side of the air line, thus these two modes can be excited at 2,500 Hz as SWs. The insets in Fig. 1d–e show the eigenmode fields of the mode 0 and mode 1 at 2,500 Hz. Because the GIMs start with low refractive indices (close to that of air), they naturally provide impedance matching between air and the GIM. The SW is further allowed to propagate in GIMs due to the gradually increased relative refractive index, since a higher refractive index indicates a better confined SW [27,28]. For the acoustic wave traveling to the left, the relative refractive index of the GIMs is greater than 1 at the opening of the waveguide. In this case, the waveguide with GIMs supports mode 0 and mode 1 of the SWs at 2,500 Hz. However, because wavenumber k_x along the x direction is significantly greater than k_0 at 2,500 Hz and above (i.e., the dispersion curve is on the far right side of the air line), there is a large momentum mismatch between the GIMs and air, giving rise to strong acoustic reflection. Very little energy is converted to that of the SW and additionally, the SW gradually attenuates as the relative refractive index of the GIMs decreases, which can be explained by the ray theorem [25]. As a result, acoustic waves traveling to the left will exhibit low transmission and these traveling to the right will exhibit high transmission, albeit in the form of SW.

In order to verify the asymmetric wave propagation illustrated in Fig. 1, we simulate the instantaneous acoustic pressure fields in Fig. 2 at 2,500 Hz. The parameters are as follows: d is 10 mm, w is 50 mm, k is 0.2 k_0, and the length of the waveguide L is 500 mm. According to Eq. (1), the relative refractive index of the GIMs gradually increases from 1 to 6. The left and right boundaries are reflectionless boundaries. In Fig. 2a, b, a point acoustic source is located inside the waveguide at 2/3L to the left end. It can be observed that the acoustic wave coming from the point source radiates along + x direction only. On the other hand, the acoustic wave propagates in both directions (Fig. 2b) without the GIMs. Similarly, when an acoustic plane wave incidents the waveguide from the left or right, the asymmetric acoustic wave transmission is demonstrated in Fig. 2c, d. In particular, the conversion from the bulk wave to SW is evident in Fig. 2c.

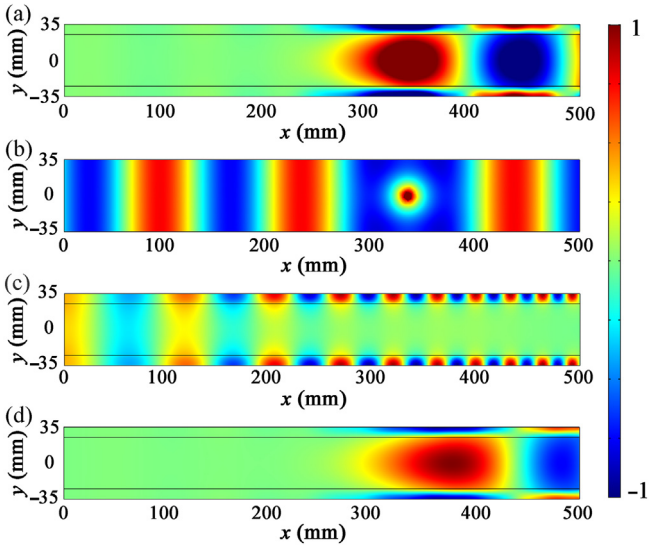

Fig. 2. The ideal asymmetric acoustic wave transmission in a waveguide. (a), (b) The simulated acoustic field for a point acoustic source inside a waveguide with (a) and without (b) GIMs at 2500 Hz. (c), (d) The simulated acoustic field for the acoustic waves incident from the left port (c) and right port (d) at 2,500 Hz.

2.2. Unit cell design and simulations results

To realize asymmetric acoustic wave transmission, a practical design of the GIM is needed. One major challenge for the design is to achieve a large relative refractive index, such as 6 used in the simulation above. From Eq. (1), it is found that either increasing d or decreasing x would reduce the largest relative refractive index required for the design. Therefore, we propose the dimensions of the GIMs as follow: d = 22 mm, L = 400 mm, w = 50 mm and k_0 = 0.2 k. In Fig. 3d, we show the ideal relative refractive indices from 1 to 2.82 as a function of x governed by Eq. (1). The unit cell structure can be found in the inset of Fig. 3d, which consists of four long arms and eight short arms. The lengths of the long arm and short arm are l and s, respectively, and the width of the arm is t. The p and h are the periods along x and y directions. In addition, p = 10 mm, h = 11 mm and t = 0.5 mm. To fabricate the sample, the material used is photopolymer resin, which density $\rho = 1300\ \mathrm{kg/m^3}$ and speed of sound $c = 716$ m/s. l and s are optimized to design the unit cell and realize the relative refractive index required by the GIMs.

In Fig. 3a, b, we sweep l (a) and s (b) to obtain the needed relative refractive index. In Fig. 3a, we show the relationship between the relative refractive index and relative impedance of the proposed unit cell with the long arm length l, which varies from 0.5 to 9.75 mm at 2,500 Hz. Here, t = 0.5 mm and s = 0.5 mm. When l is increased, the relative refractive index grows slowly at the beginning and then increases fast. The maximum relative refractive index is 2.15. Larger long arm lengths are not trialed because they would be close to the period of the structure p. To further increase the relative refractive index, s is treated as a variable in Fig. 3b, which varies from 1.15 to 3.5 mm at 2,500 Hz. Here, t = 0.5 mm and l = 9.75 mm. In this case, the relative refractive index increases from 2.15 to 3.55 as s rises. In addition, the relative refractive index and relative impedance of the proposed unit cell over the frequency span from 1,500 to 3,500 Hz, where t = 0.5 mm, l = 9.75 mm and s = 3.5 mm are shown in Fig. 3c. The relative refractive index changes relatively slow as frequency increases. By optimizing the long arm length l and short arm length s, we obtain the unit cells that would provide the required indices as shown in Fig. 3d and the detailed sizes of the 40 unit cells (No. 1–40) are shown in Table 1. Meanwhile, the gradually increased impedances of the unit cells in +x direction greatly facilitate the propagation of acoustic surface mode with low reflection loss.

To prove the asymmetric acoustic waves transmission, we use the unit cells designed in Fig. 3 to compose the GIMs in Fig. 1. Similar to the Fig. 2c, d, full-waves simulations was conducted to observe the acoustic pressure field in Fig. 4, and the simulated conditions are the same with Fig. 2c, d. From the dimensions of the GIMs, we propose 40 layers of unit cells along x direction and 2 layers of unit cells along y direction to build the GIMs. For the acoustic waves coming from the left, the acoustic waves are gradually converted into SWs (Fig. 4a) and reach the right end of the waveguide. For the acoustic waves coming from the right, the acoustic waves are blocked at some positions and most of the acoustic waves cannot pass through the waveguide (Fig. 4b).

2.3. Experimental results

To experimentally validate the asymmetric acoustic waves transmission of the waveguide with GIMs using a home-built acoustic near-field scanning system, we fabricate a sample, comprising two identical GIMs and aluminum plates which are

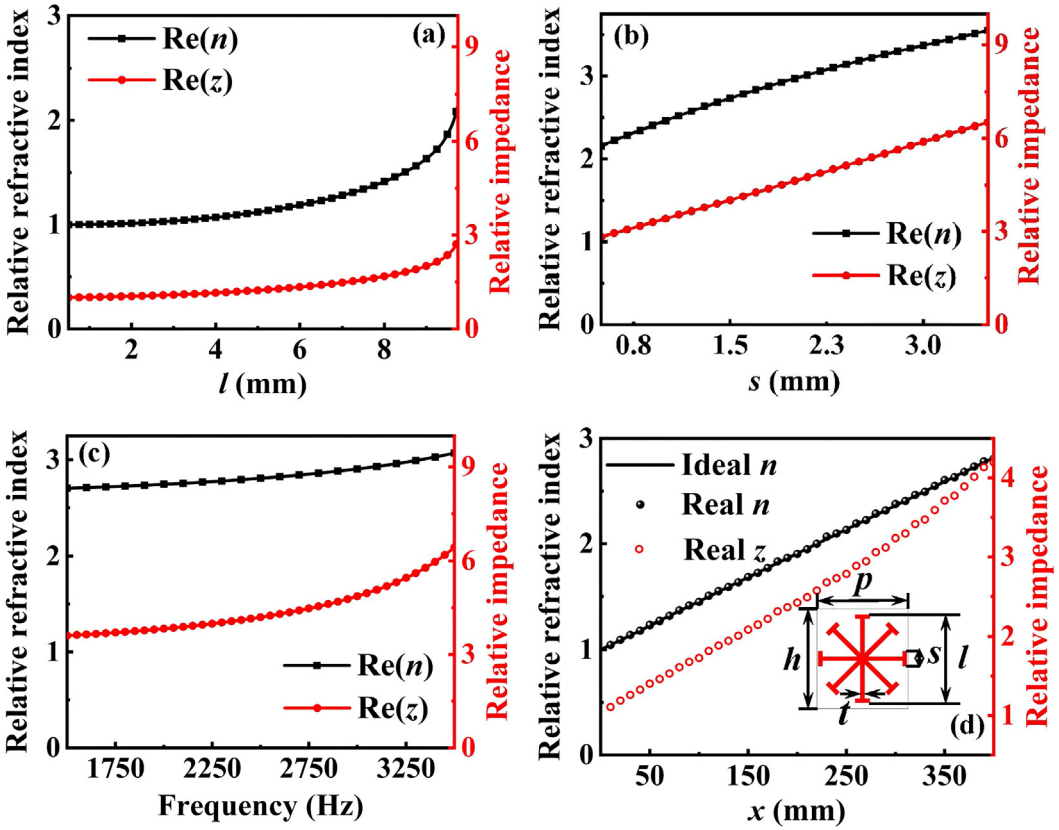

Fig. 3. Design of the proposed unit cells. (a) The relationship between the relative refractive index and relative impedance of the proposed unit cells with the long arm *l*, which varies from 0.5 to 9.75 mm at 2,500 Hz. Here, $t = 0.5$ mm and $s = 0.5$ mm. (b) The relationship between the relative refractive index and relative impedance of the proposed unit cells with the short arm s, which varies from 1.15 to 3.5 mm at 2,500 Hz. Here, $t = 0.5$ mm and $l = 9.75$ mm. (c) The relative refractive index and relative impedance of the proposed unit cells from 1,500 to 3,500 Hz. Here, the dimensions of the unit cells as follow: $t = 0.5$ mm, $l = 9.75$ mm and $s = 3.5$ mm. (d) The ideal relative refractive index for the GIMs and the corresponding attainable relative refractive index and impedance from the proposed real unit cells. The inset is the proposed unit cell of the GIMs.

Table 1
The detail sizes of the proposed unit cells.

No.	*l* (mm)	s (mm)	No.	*l* (mm)	s (mm)
1	3.3	0.5	21	9.6	0.5
2	4.5	0.5	22	9.65	0.5
3	5.3	0.5	23	9.7	0.5
4	5.9	0.5	24	9.72	0.5
5	6.5	0.5	25	9.74	0.5
6	6.9	0.5	26	9.75	0.55
7	7.3	0.5	27	9.75	0.6
8	7.7	0.5	28	9.75	0.7
9	8	0.5	29	9.75	0.75
10	8.2	0.5	30	9.75	0.85
11	8.5	0.5	31	9.75	0.9
12	8.7	0.5	32	9.75	1
13	8.85	0.5	33	9.75	1.05
14	9	0.5	34	9.75	1.15
15	9.15	0.5	35	9.75	1.25
16	9.25	0.5	36	9.75	1.3
17	9.35	0.5	37	9.75	1.4
18	9.45	0.5	38	9.75	1.5
19	9.5	0.5	39	9.75	1.6
20	9.55	0.5	40	9.75	1.65

considered as PRB as shown in Fig. 5a. The geometric and material parameters of the GIMs samples are the same as those in Fig. 4, which are fabricated via 3D printing. The height of the GIMs sample is 12 mm, which is deposited on a 2 mm thick photopolymer resin plate. The aluminum plates with 12 mm height are manufactured via computerized numerical control (CNC) machine. In Fig. 5a, the near-field scanning system is a planar waveguide which consists of two parallel plexiglass plates (the upper plexiglass plate is not shown in the figure). In order to avoid unnecessary scattering at the left and right boundaries, we place acoustic absorbing forms at the left and right ends. A 1/4 in. microphone (BSWA MPA 416) is embedded into the upper plate to detect acoustic pressure field at various locations, and the signals of the microphone are transmitted into the computer for post-processing. A loudspeaker is placed at the entry of the waveguide to generate acoustic waves with 2,500 Hz frequency. When the acoustic waves coming from the left port, the location of the GIMs samples and the loudspeaker are shown in Fig. 5a. For the acoustic waves coming from the right port, the loudspeaker is placed in the right port and the location of the GIMs samples does not change. A translation stage is used to carry the upper plexiglass plate and scans in *x* and *y* directions. The acoustic pressure fields could be measured in a certain area as the red dash box shown in Fig. 5a. The step resolution in both directions is 2 mm.

In Fig. 5b, c, we show the measured acoustic pressure fields for the acoustic waves from the left and right ports at 2,500 Hz. In Fig. 5b, the acoustic waves propagate along *x* direction and are smoothly converted to SWs. For the acoustic waves from the right port, the acoustic waves gradually attenuate and are blocked at some positions (Fig. 5c), validating the asymmetric acoustic wave transmission effect. It is noteworthy that there is slight difference between the simulated results (Fig. 4) and the measured results (Fig. 5b, c). This is mainly because when we scan the acoustic pressure fields, there is a 1 mm air gap between the sample and the upper plexiglass plate. The air gap is used to facilitate the microphone detection while preventing damage to the sample. Such

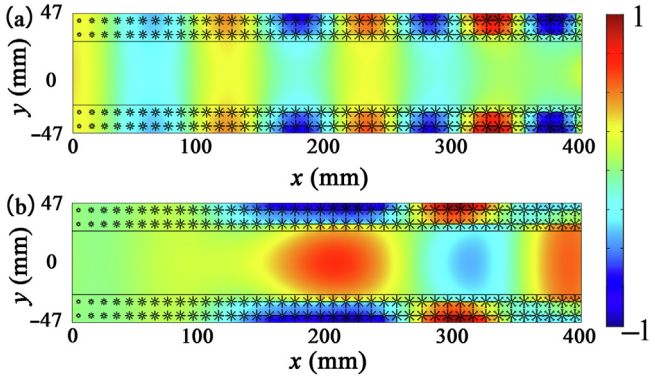

Fig. 4. The simulated acoustic fields for the acoustic waves incident from the left port (a) and the right port (b) at 2,500 Hz using the real unit cells, where L = 400 mm, w = 50 mm and d = 22 mm.

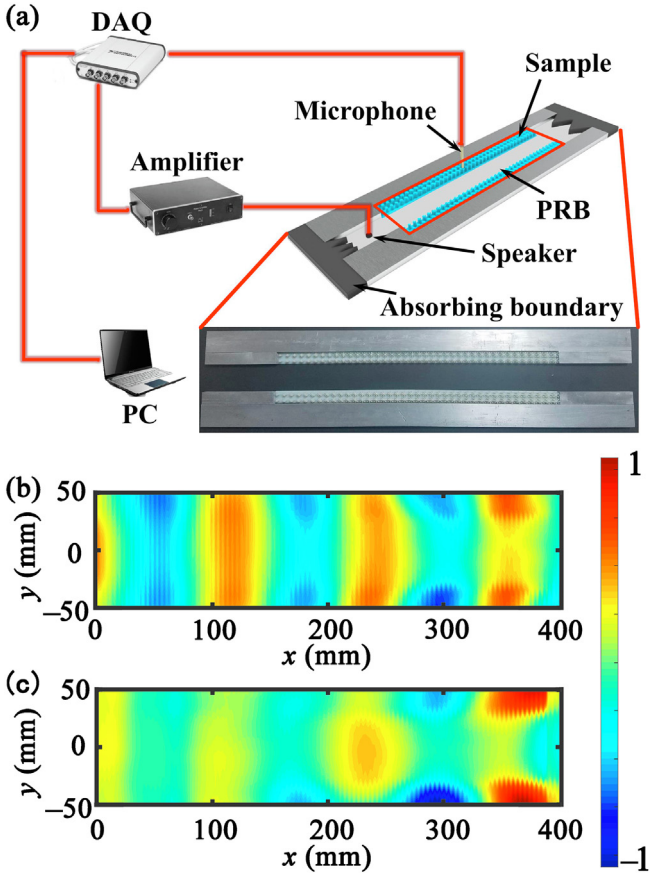

Fig. 5. The experimental setup and the measured results. (a) Experimental setup for mapping the acoustic pressure field of the asymmetric acoustic wave transmission. The red dash box is the measured area. The inset is the photograph of the fabricated GIMs samples and the waveguide composed by aluminum plates which are considered as PRB. (b), (c) The measured results for the acoustic waves from the left port (b) and right port (c) at 2,500 Hz.

air gap causes energy leakage and the relative refractive index and dispersion relations of the unit cells can be different from the design during the measurement. Nevertheless, asymmetric acoustic wave transmission is still evident from the measurement.

3. Conclusions

In summary, we have numerically and experimentally demonstrated asymmetric acoustic wave transmission through a waveguide with GIMs. We show that the acoustic waves could be converted into SWs when they come from the left side of the waveguide and is further allowed to be transmitted through the waveguide. On the other side, the wave cannot propagate when they come from the right side of the waveguide. It is demonstrated that surface wave conversion could be a useful tool to control acoustic waves and new acoustic devices can be designed and fabricated. Our study provided a means to control the transmission of the sound, added new applications of surface waves in the acoustic domain, and meanwhile opened a new avenue for high-efficiency acoustic couplers and noise control. In addition, several methods can be employed to achieve tunable metamaterials and metasurfaces [29]. We think it is really an important trend for developing the high efficiency one way transmission device.

Conflict of interest

The authors declare that they have no conflict of interest.

Acknowledgments

This work was supported by the National Key Research and Development Program of China (2017YFA0700201, 2017YFA0700202, and 2017YFA0700203), the National Natural Science Foundation of China (61631007, 61571117, 61138001, 61371035, 61722106, 61731010 and 11227904), and the 111 Project (111-2-05).

Author contributions

W-K Cao conceived the original idea, performed the numerical calculations and designed the experiments; L-T Wu, C Zhang and J-C Ke analyzed the results; W-K Cao, Q Cheng, T-J Cui and Y J prepared the manuscript; All authors contributed to the discussions.

References

[1] García-Chocano VM, Christensen J, Sánchez-Dehesa J. Negative refraction and energy funneling by hyperbolic materials: an experimental demonstration in acoustics. Phys Rev Lett 2014;112:144301.
[2] Kaina N, Lenmoult F, Fink M, et al. Negative refractive index and acoustic superlens from multiple scattering in single negative metamaterials. Nature 2015;525:77.
[3] Shen C, Xie Y, Sui N, et al. Broadband acoustic hyperbolic metamaterial. Phys Rev Lett 2015;115:254301.
[4] Sui N, Yan X, Huang T, et al. A lightweight yet sound-proof honeycomb acoustic metamaterial. Appl Phys Lett 2015;106:171905.
[5] Li J, Wang W, Xie Y, et al. A sound absorbing metasurface with coupled resonators. Appl Phys Lett 2016;109:091908.
[6] Li J, Fok F, Yin X, et al. Experimental demonstration of an acoustic magnifying hyperlens. Nat Mater 2009;8:931.
[7] Zhu Y, Fan X, Liang B, et al. Ultrathin acoustic metasurface-based schroeder diffuser. Phys Rev X 2017;7:021034.
[8] Jiménez N, Cox TJ, Romero-García V, et al. Metadiffusers: deep-subwavelength sound diffusers. Sci Rep 2017;7:5389.
[9] Jiang X, Li Y, Liang B, et al. Convert acoustic resonances to orbital angular momentum. Phys Rev Lett 2016;117:034301.
[10] Zigoneanu L, Popa BL, Cummer SA. Three-dimensional broadband omnidirectional acoustic ground cloak. Nat Mater 2014;13:352.
[11] Fleury R, Sounas D, Alù A. An invisible acoustic sensor based on parity-time symmetry. Nat Commun 2015;6:5905.
[12] Gu Z, Hu J, Liang B, et al. Broadband non-reciprocal transmission of sound with invariant frequency. Sci Rep 2016;6:19824.
[13] Popa BL, Cummer SA. Non-reciprocal and highly nonlinear active acoustic metamaterials. Nat Commun 2014;5:3398.
[14] He Z, Peng S, Ye Y, et al. Asymmetric acoustic gratings. Appl Phys Lett 2011;98:083505.
[15] Zhu Y, Zou X, Liang B, et al. Acoustic one-way open tunnel by using metasurface. Appl Phys Lett 2015;107:113501.
[16] Li Y, Shen C, Xie Y, et al. Tunable asymmetric transmission via lossy acoustic metasurfaces. Phys Rev Lett 2017;119:035501.
[17] Shen C, Xie Y, Li J, et al. Asymmetric acoustic transmission through near-zero-index and gradient-index metasurfaces. Appl Phys Lett 2016;108:223502.

[18] Jiang X, Liang B, Zou X, et al. Acoustic one-way metasurfaces: asymmetric phase modulation of sound by subwavelength layer. Sci Rep 2016;6:28023.
[19] Ge Y, Sun H, Yuan S, et al. Broadband unidirectional and omnidirectional bidirectional acoustic insulation through an open window structure with a metasurface of ultrathin hooklike meta-atoms. Appl Phys Lett 2018;112:243502.
[20] Liang B, Guo X, Tu J, et al. An acoustic rectifier. Nat Mater 2010;9:989.
[21] Zhu Y, Zou X, Liang B, et al. Broadband unidirectional transmission of sound in unblocked channel. Appl Phys Lett 2015;106:173508.
[22] Zhu J, Chen Y, Zhu X, et al. Acoustic rainbow trapping. Sci Rep 2013;3:1728.
[23] Xu Y, Fu Y, Chen H. Planar gradient metamaterials. Nat Rev Mater 2016;1:16067.
[24] Sun S, He Q, Xiao S, et al. Gradient-index meta-surfaces as a bridge linking propagating waves and surface waves. Nat Mater 2012;11:426–31.
[25] Xu Y, Gu C, Hou B, et al. Broadband asymmetric waveguiding of light without polarization limitations. Nat Commun 2013;4:2561.
[26] Wu L, Song G, Cao W, et al. Generation of multiband spoof surface acoustic waves via high-order modes. Phys Rev B 2018;97:214305.
[27] Cao W, Wu L, Zhang C, et al. Acoustic surface waves on three-dimensional groove gratings with sub-wavelength thickness. Appl Phys Express 2018;11:087301.
[28] Ding Y, Statharas EC, Yao K, et al. A broadband acoustic metamaterial with impedance matching layer of gradient index. Appl Phys Lett 2017;110:241903.
[29] Nemati A, Wang Q, Hong M, et al. Tunable and reconfigurable metasurfaces and metadevices. Opto-Electron Adv 2018;1:180009.

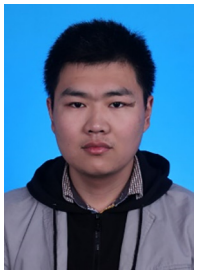

Wenkang Cao received the B.S. degree in Material Forming and Control Engineering from Nanchang Hangkong University in 2013, the M.S. degree in Materials Science and Engineering from Naval University of Engineering in 2016, and is currently pursuing the Ph.D. degree in Southeast University. His current research interests include acoustic metamaterials and metasurfaces.

Qiang Cheng received the B.S. and M.S. degrees from the Nanjing University of Aeronautics and Astronautics in 2001 and 2004, respectively, and the Ph.D. degree from Southeast University in 2008. In 2008, he joined the State Key Laboratory of Millimeter Waves, Southeast University, where he was involved in the development of metamaterials and metadevices. He leads a group of Ph.D. students and master students in the area of metamaterials, tunable microwaves circuits, microwave imaging, and terahertz systems.

Tie-Jun Cui received his doctorate from Xidian University, China in 1993. He was an Alexander von Humboldt Foundation Research Fellow at the University of Karlsruhe, Germany (2005–2007), a Postdoctoral Research Associate (1997–2000) and Research Scientist (2001–2002) at the University of Illinois at Urbana-Champaign, USA. In 2002, he joined the Department of Radio Engineering, Southeast University, China, as Cheung-Kong Professor. His research interests include metamaterials, plasmonics in microwaves, and computational electromagnetics.

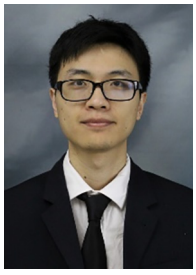

Yun Jing received his B.S. degree in electronic science and engineering from Nanjing University in 2006 and M. S. degree from Rensselaer Polytechnic Institute in 2007. He received his Ph.D. degree in architectural acoustics from Rensselaer Polytechnic Institute in 2009. Prior to joining the North Carolina State University in 2011, he was a research fellow at Brigham and Women's Hospital, Harvard Medical School. He was promoted to tenured Associate Professor in 2017. He is interested in biomedical ultrasound, acoustic metamaterials, architectural acoustics, nonlinear acoustics and noise control.